Adaptive Embedded LES of the NASA Hump

Stephen Woodruff *
NASA Langley Research Center, Hampton, VA 23681

A scheme for adaptive embedded LES is proposed which automatically determines boundaries for LES regions in a hybrid LES-RANS computation, with the goal of minimizing the LES part of the computation for maximum accuracy with minimum cost. The model-invariant hybrid formulation enables this scheme through greater flexibility in the placement of RANS-LES transitions. An adaptive embedded large-eddy simulation is carried out for the NASA hump test case and adaptive meshing is added to show how additional adaptive features may be controlled by the adaptive hybrid scheme.

I. Introduction

The relative speed of Reynolds-Averaged Navier-Stokes (RANS) computations and the relative accuracy of Large-Eddy Simulations (LES) has made the prospect of combining them for maximum speed and accuracy an enticing one for a long time. By far the most successful combinations to date have been Detached-Eddy Simulation (DES)[1] and Wall-Modeled LES (WMLES),[2] but problems such as uncertainties during RANS-LES transitions ("grey areas") and cases that lead to unexplained poor results persist (e.g., Refs. 1, 3).

In an effort to clarify this situation and, ultimately, allow greater freedom in defining RANS and LES regions, the model-invariant hybrid formulation was developed.[4–7] By focusing on how meaningful physical information may be extracted from a computation, even in the midst of a RANS-LES transition, this formulation shows how "grey" areas may be eliminated. In the process, it reveals that terms must be added to the governing equations to restore the physical balances disturbed by the model changes during a RANS-LES transition. These terms help to manage RANS-LES transitions more accurately, and thus represent a powerful tool for hybrid computations, permitting much more freedom in placing the boundaries of the RANS and LES regions.

The natural use of this new freedom is in embedded LES (e.g., Ref. 8), where LES is performed only in those regions where RANS fails (such as a separated-flow region); RANS is performed everywhere else for maximum efficiency. To determine, in any given problem, which regions must be solved by LES and what their boundaries are, an adaptive embedded LES approach is proposed here, where trial boundaries are expanded until the solutions are no longer sensitive to the boundary position. The approach is then combined with adaptive meshing and demonstrated for the NASA hump test case.[9]

While DES and WMLES have been widely used and have enjoyed a great deal of success, the nature of the LES-RANS transition in these approaches, and how problems in the transition contribute to the failures of these techniques in many important problem areas, have received only limited attention. There have been, however, some systematic investigations into how to manage the LES-RANS transition in hybrid computations that should be mentioned before proceeding.

A number of authors, including Germano,[10] Sanchez-Rocha and Menon[11,12] and Rajamani and Kim,[13] have proposed hybrid formulations in which the flow variables are defined by explicit filters, usually a blend of RANS and LES filters. These formulations lead to additional terms being included in the governing equations for which models are constructed,[11,12] or which are determined by inverse filtering.[13] Wallin and Girimaji[14] have also presented a formulation in which additional terms in the governing equations compensate for changes in the blending parameter controlling the mix of RANS and LES model at a point in the flow; these terms are modelled with eddy-viscosity expressions. Medic et al.[15] and Breuer et al.[16] modify the RANS eddy viscosity to account for resolved stresses; Wang and Moin[17] incorporate a similar strategy into one of their wall models.

*Research Scientist, Computational AeroSciences Branch

Fitting the LES-RANS transition to specific parts of the flow, through the use of prescribed blending functions, or matching RANS and LES regions at specific points in the boundary layer, has met with some success. The former has been employed by Shur et al.[18] in the IDDES variation of DES and the latter has been used by Edwards and coworkers.[19,20]

Stochastic forcing, and filtering, have been used to manage and control LES-RANS transitions. Hamba[21] has derived derivative expressions similar to those used here in terms of an explicit filtering operation. Keating et al.[22] have used stochastic forcing and a feedback loop to try to make RANS-to-LES transitions more rapid and accurate.

In the following section, details of the NASA hump separated-flow problem are given and the numerics used to solve it are described. Then details of the model-invariant formulation for hybrid LES-RANS compuations are given, followed by its application to embedded LES, adaptive embedded LES and adaptive embedded LES with grid adaption. Results from each of these approaches applied to the NASA hump test case follow. The paper concludes with a discussion of the opportunities opened up by the model-invariant formulation for hybrid computations.

II. Problem Definition and Numerics

The NASA hump (half airfoil) experiment[9] provides a separated-flow test case for the adaptive embedded LES computation. The computational domain is shown in Figure 1; flow separates on the aft portion of the airfoil surface on the lower boundary and reattaches at approximately $x/c = 1.11$. (The chord of the airfoil is denoted by c, x and y are streamwise and normal coordinates, respectively, with origin at the airfoil leading edge.) The upper and lower boundaries of the computational domain are solid walls, there is uniform inflow at the left boundary and the standard incompressible-flow convective outflow condition[23] is employed at the right boundary. The flow is assumed periodic in the spanwise direction (out of the page) and the span is $0.2c$.

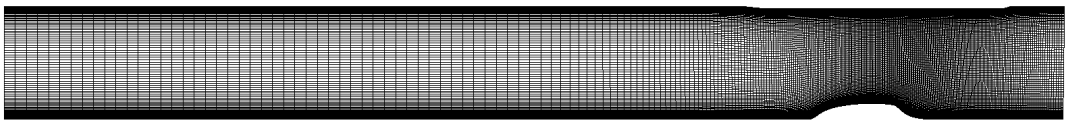

Figure 1. Computational domain and initial grid.

There are a number of indications that the boundary layer upstream of the hump in the experiments is not a canonical flat-plate boundary layer (see, for example, the discussion in the Appendix of Ref. 24), which makes reproducing the experimental conditions in an eddy-resolving computation particularly difficult. Curiously, this was found in the present work (as in some previous work, such as[25]) to be much less of an issue the closer the inflow RANS-to-LES transition is to the separation point and so no special measures are taken here to address this problem.

The incompressible Navier-Stokes equations are solved in conjunction with the Menter SST turbulence model,[26] converted to a hybrid model after the fashion of Strelets,[27] except that here the transition is much more gradual (see below). The model-invariance terms described in the following section are included in these equations. The equations are discretized by fourth-order central diffrences in the x and y directions and are discretized spectrally in the spanwise direction. Sixth-order filtering[28] is employed for numerical stabilization. A second-order time-advancement scheme is employed with Newton subiterations (following Ref. 29).

The grid of Figure 1 (Grid A) is employed in the embedded LES computation. It has 304 points in the streamwise direction, 128 points in the vertical direction and 20 spanwise modes are used. The points nearest the wall are at a y^+ of approximately 1. This grid is similar to one employed successfully in previous model-invariant computations of the NASA hump in a DES or wall-modeled LES configuration.[7] A second

grid (Grid B) was employed in the adaptive computations. It covers the same computational domain and has the same number of points, but the points in the vertical direction are redistributed so the point nearest the wall is at $y^+ \approx 2$, to permit larger time steps while maintaining residual reduction.

III. Adaptive Embedded LES

In this section, the ingredients of the adaptive embedded LES computation with grid adaption are described. The essential role of the model-invariance formulation is discussed first, then it is shown how the adaptive embedded LES capability and the grid adaption capability are simple extensions once the machinery of the model-invariance formulation is available.

III.A. Model-Invariant Embedded LES

If one imagines a flow variable like the velocity $\mathbf{v}$ to be a function of time, space and the blending parameter λ, $\mathbf{v} = \mathbf{v}(t, \mathbf{x}, \lambda(t, \mathbf{x}))$, then the fact that λ is, in a hybrid computation, also a function of space and time implies derivatives of $\mathbf{v}$ have two contributions. The gradient of $\mathbf{v}$, for example,

$$\nabla \mathbf{v} = \nabla_x \mathbf{v} + \mathbf{v}_s \nabla \lambda \tag{1}$$

now involves the gradient of $\mathbf{v}$ with respect to $\mathbf{x}$ and a term representing the change in the flow variable due to the change in the hybrid LES-RANS blended model controlled by the blending parameter λ. (It is notationally convenient here and below to represent derivatives with respect to the third argument [the blending parameter] of flow variables like $\mathbf{v}$ as $\mathbf{v}_s$. The operator ∇_x represents the gradient with respect to the second argument.)

The second term on the right of Equation 1, while representing a real effect, is not part of the physical gradient of $\mathbf{v}$ and thus represents an error when the full derivative of Equation 1 is used in the governing equations. This is not simply a technical difficulty, but rather a fundamental physical error in the way hybrid LES-RANS computations are traditionally formulated. The nature of this error, and how it may be eliminated in a systematic way to dramatically improve hybrid capabilities, is the topic of this section.

III.A.1. Overview

The model-invariant formulation for hybrid LES-RANS computations was developed to provide a fundamental basis for understanding and improving the behavior of hybrid LES-RANS computations in transitional regions between LES and RANS. It is based on the essential observation that physical quantities cannot depend on the hybrid model blending parameter; they are *model invariant*. (Specifically, physical quantities are invariant under model changes within the one-parameter family of models specified by a given blended hybrid LES-RANS model and parametrized by the blending parameter.) Since individual quantities in the computation, such as the modelled turbulent kinetic energy and the resolved turbulent kinetic energy, do depend strongly on the blending parameter (i.e, energy shifts from modelled to resolved fields during a RANS to LES transition), this turns out to be a significant constraint. Terms are added to the Navier-Stokes and turbulence-model equations that remove the spurious gradients in these quantities due to blending-parameter dependence and so restore the physical balances in the equations.

These additional terms involve *model sensitivities*, the response of the flow variables to changes in the blending parameter. The model sensitivities satisfy equations derived from the Navier-Stokes and turbulence-model equations, but a simple approximation to the solutions of those equations for the model sensitivities is employed in the present work. The approximation has three components: a) a contribution based on equilibrium (production equals dissipation) considerations; this contribution corrects log-layer mismatch, for example; b) a contribution that injects fluctuations to aid the transition from RANS to LES, particularly when turbulence is convected from a RANS region into an LES region; and c) a contribution that removes fluctuations, such as when turbulence is convected from LES regions to RANS regions.

This approximation for the model sensitivities, when combined with gradual transitions between RANS and LES regions (in contrast to the rapid transitions favored by other hybrid approaches), has, in the flows attempted so far, been successful in permitting RANS-LES transitions to be placed almost arbitrarily across attached boundary layers (e.g., Ref. 5). Thus, one may perform embedded LES after the fashion shown in Figure 2, where the lines show (schematically) the inner and outer boundaries of the gradual transition

between RANS and LES and the LES "box" has been positioned so the inflow boundary is upstream of separation and the outflow boundary is well downstream of reattachment.

III.A.2. Model Invariance and the Governing Equations

This section is essentially a demonstration that if the mean flow variables are to retain their physical values throughout LES-RANS transition zones, new terms must be added to the governing equations to compensate for the unphysical effects of switching between RANS and LES models within a computation.

As noted above, the incompressible Navier-Stokes equations will be solved with a variation on Strelets' DES model[27] based on the Menter SST turbulence model equations.[26] The governing equations then take the form

$$\begin{aligned} \nabla \cdot \mathbf{v} &= 0 \\ \partial_t \mathbf{v} + (\mathbf{v} \cdot \nabla)\mathbf{v} &= -\nabla p + \nabla \left[\left(\frac{1}{Re} + \nu_t \right) \nabla \mathbf{v} \right] \\ \partial_t k + (\mathbf{v} \cdot \nabla) k &= P - \epsilon + \nabla \cdot \left[\left(\frac{1}{Re} + \sigma_k \nu_t \right) \nabla k \right] \\ \partial_t \omega + (\mathbf{v} \cdot \nabla)\omega &= \frac{\gamma}{\nu_t} P - \beta \omega^2 + \nabla \cdot \left[\left(\frac{1}{Re} + \sigma_\omega \nu_t \right) \nabla \omega \right]. \end{aligned} \tag{2}$$

Here, $\mathbf{v}$ is the resolved velocity field and p is the resolved pressure. The Reynolds number and eddy viscosities are Re and ν_t, respectively. The turbulence production is $P = \nu_t S_{ij} S_{ij}$, where S_{ij} is the rate-of-strain tensor.

To create the blended hybrid model, the dissipation, ϵ, is (following Strelets) expressed in terms of a hybrid length scale ℓ_H: $\epsilon = k^{3/2}/\ell_H$. Strelets switches ℓ_H instantaneously between the RANS length scale $\ell_{\text{RANS}} = k^{1/2}/\omega$ and the LES length scale $\ell_{\text{LES}} = C_{DES}\Delta$. Here, in contrast, a gradual change between the two is provided by the blending parameter λ according to

$$1/\ell_H = (1-\lambda)/\ell_{\text{RANS}} + \lambda/\ell_{\text{LES}} \tag{3}$$

This blending of the inverse length scales is tantamount to blending the RANS and LES dissipation expressions; any other choice would be perfectly acceptable to this formulation (though not necessarily to the physics).

The blending parameter λ defines the RANS and LES regions of the computational domain and the transition zones in between. It may be determined in any manner one pleases, but here it will be specified prior to the computation, with the specification ultimately becoming part of an adaptive process.

The purpose of the model-invariant formulation is to control precisely the transition between LES and RANS solutions in a hybrid computation. This is achieved by identifying quantities that are common between LES and RANS and ensuring that these quantities maintain physically-correct values throughout the LES-RANS transition. The "grey area" is consequently eliminated and a physically meaningful solution is computed throughout the computational domain.

The quantities in question are, of course, the Reynolds averages of the flow variables: they are the only quantities explicitly available from the RANS solution, and one's expectation is that the Reynolds average (to be denoted $\langle \cdot \rangle$) of an LES flow variable (or any blend of RANS and LES) should, ideally, give the RANS solution: e.g., $\langle \mathbf{v} \rangle$ gives the same result for any value of λ. This is what is customarily expected when LES or hybrid LES-RANS variables are averaged to yield mean quantities that are compared with experiment or other computations.

To see the consequences to a hybrid computation of imposing the condition that RANS averages of the flow variables be independent of λ, consider first the case of a computation where the blending parameter is equal to a constant value, s, throughout the flow domain: $\lambda = \text{const.} = s$. This is not proposed as a viable way to carry out a flow computation (though Girimaji and coworkers have had some success with a related approach, e.g. Ref. 30); it is merely an instructive first step in understanding what happens in a fully hybrid computation with λ varying from 0 to 1 in the flow domain. The model-invariance condition in this restricted case is then, for the velocity, $\langle \mathbf{v} \rangle = \text{const.}$ for all s, or $\langle \mathbf{v}_s \rangle = 0$, and similarly for the other flow variables.

Differentiating Equations 2 with respect to s yields a system of linear equations for the s-derivatives of the flow variables. Applying the Reynolds average to these equations, one finds the linear terms yield time and space derivatives of $\langle \mathbf{v}_s \rangle$ and $\langle p_s \rangle$, which should be zero according to the model-invariance condition.

The remaining, nonlinear, terms then yield additional conditions which must be satisfied in order that a computation be model invariant. The momentum equation thus becomes

$$\begin{aligned}\rho\partial_t\langle\mathbf{v}_s\rangle - \nabla\langle p_s\rangle + \nabla\frac{1}{Re}\nabla\langle\mathbf{v}_s\rangle &= \langle -(\mathbf{v}\cdot\nabla)\mathbf{v} + \nabla\nu_t\nabla\mathbf{v}\rangle_s \\ &= \nabla\cdot\langle -\mathbf{v}\mathbf{v} + \nu_t\nabla\mathbf{v}\rangle_s. \end{aligned} \tag{4}$$

The model-invariance condition implies that the left-hand side of this equation is zero and so the right-hand side must also be zero, implying that $\langle -\mathbf{v}\mathbf{v}+\nu_t\nabla\mathbf{v}\rangle$ is also a model invariant. This makes sense intuitively: it simply means the resolved Reynolds stress and the modeled stress should combine to give the total Reynolds stress regardless of whether one is doing RANS, LES or something in between. The corresponding expression for the trace of the Reynolds stress, stating that the total kinetic energy is the combination of the resolved and modeled kinetic energies, is perhaps even more intuitive: $\langle\mathbf{v}\cdot\mathbf{v}/2+k\rangle_s = 0$. These new model invariants will be referred to as secondary model invariants.

The intuitive reasonableness of the secondary model invariants involving the nonlinear terms of the governing equations notwithstanding, whether they are satisfied by any given blended hybrid model composed of a particular RANS model, a particular LES model and a particular scheme for blending the two is not by any means guaranteed. The failure of many RANS models to produce accurate solutions for the turbulent kinetic energy, for example, is well known (see, for example, Ref. 31) and makes the accuracy of even the intuitively appealing turbulent kinetic energy model invariant of the previous paragraph dubious. This is an issue that needs to be addressed, with the goal of developing blended hybrid LES-RANS models that do in fact satisfy the model-invariance conditions. As will be seen in the following, the model-invariance framework outlined here plays a vital role in maintaining model invariance in a hybrid computation, but the accuracy with which it does so is limited by the accuracy with which the underlying blended model satisfies the secondary invariance conditions. Fortunately, previous experience suggests even existing models work fairly well[4–7] and the results presented below bear this out.

The above analysis may be repeated for the case of a blending parameter that depends on time and space, $\lambda = \lambda(t,\mathbf{x})$. In fact, use of a functional derivative with respect to $\lambda(t,\mathbf{x})$ makes the analysis almost identical, but an alternative approach will be employed here due to functional-derivative manipulations being not so widely known.

Consider, then, what happens if a computation with a variable blending parameter $\lambda = \lambda(t,\mathbf{x})$ experiences a small perturbation: $\lambda(t,\mathbf{x}) \to \lambda(t,\mathbf{x})+\varepsilon\eta(t,\mathbf{x})$, $\varepsilon \ll 1$, $\eta = O(1)$. The flow variables will be correspondingly perturbed; for example, the velocity becomes $\mathbf{v} = \mathbf{v}^0 + \varepsilon\mathbf{v}^1 + \ldots$ and the perturbations $\mathbf{v}^1$, p^1, etc., satisfy linear equations that may be found by substituting the perturbation series into Equations 2. The model-invariance condition may here be interpreted as a robustness condition: that $\langle\mathbf{v}\rangle$ should, to the appropriate order, be independent of the perturbation η, reflecting the fact that a physically meaningful computation should not be sensitive to modelling artifacts like the blending parameter. Thus, the model-invariance condition reduces to the requirement that $\langle\mathbf{v}^1\rangle$ and the perturbations of the other model invariants be zero.

The equations for the perturbations $\mathbf{v}^1$, p^1, etc., are almost the same as the equations for $\mathbf{v}_s$, p_s, ... in the previous analysis. The difference is the presence of the arbitrary function of time and space $\eta(t,\mathbf{x})$. Attempting to follow the steps of the previous analysis, there is in principle no difficulty in solving the perturbation equations for the perturbed flow variables for arbitrary η, but problems arise when the Reynolds average of the perturbed equations are taken and the model-invariance condition is imposed. Specifically, the secondary model invariant which explicitly contains λ, and therefore η, is that associated with the total kinetic-energy equation. (That is, the equation for the model invariant $\langle\mathbf{v}\cdot\mathbf{v}/2+k\rangle_s = 0$.) It contains terms like

$$\langle -(\beta\omega^0 k^1 + \beta k^0\omega_1)(1-\lambda) + \beta\omega^0 k^0\eta + \cdots\rangle \tag{5}$$

and it is necessary that the perturbation solution for k, ω and the other variables have the form k^1, ω^1, $\ldots \propto \eta$ in order that the invariance condition be satisfied for arbitrary η. On the other hand, this form does not satisfy the original equations for the perturbations, so model invariance is inconsistent with the governing equations.

Model invariance may be restored to the equations by modifying the time and space derivatives so that the solution required by the model-invariant conditions is also a solution of the governing equations. The modification is that introduced by Germano,[10] in the context of the explicit filtering operation he used to define the hybrid flow variables. The present analysis is more general and shows the modification is required for any hybrid computation.

The modified time and space derivatives are

$$\tilde{\partial}_t \equiv \frac{\partial}{\partial t} - \frac{\partial \lambda}{\partial t}\frac{\partial}{\partial s} \qquad \text{and} \qquad \tilde{\nabla} \equiv \nabla - (\nabla\lambda)\,\frac{\partial}{\partial s}, \tag{6}$$

which replace all the time and space derivatives in the governing Equations 2. The modifications involve terms composed of derivatives of the blending parameter λ and derivatives of the flow variables with respect to s, the variable introduced in the above analysis for a constant blending parameter. These latter quantities will be referred to as *model sensitivities*, because they reflect the sensitivity of the flow variables to changes in the hybrid turbulence model when the blending parameter is varied. The determination of the model sensitivities will be described in the following subsection.

With the modified derivatives, the solutions for the perturbed flow variables are just the corresponding solutions from the constant-blending-parameter analysis multiplied by η. For example, the velocity perturbation is $\mathbf{v}^1 = \mathbf{v}_s\eta$, and the fact that $\langle \mathbf{v}_s \rangle = 0$ has already been established implies that $\langle \mathbf{v}^1 \rangle = 0$, as was required to confirm the model invariance of $\langle \mathbf{v} \rangle$.

The above analysis shows that simply requiring that the mean flow variables retain their physically correct values throughout the LES-RANS transition imposes conditions on the turbulence model (so that the secondary invariance conditions are satisfied) and on the equations (requiring modification of the derivatives). While the secondary invariance conditions are intuitively reasonable, it is worth asking why it is acceptable to change the governing equations in the manner just described. In fact, the question is wrong: the governing equations aren't being changed, they're being changed *back*, to compensate for the change made to the equations by introducing a time- and space-dependent blending parameter.

The time- and space-varying blending parameter instantaneously changes the turbulence model from point to point and instant to instant, but it can't instantaneously make the corresponding changes in the solution: the flow evolves on time and space scales determined by its own dynamics. The resulting unphysical effects can taint the hybrid computation both in the transition region (the "grey area") and in the wider flow domain. Imposing model invariance provides the prescription for correcting these effects.

III.A.3. Model Sensitivities

The basis of the present approach for determining the model sensitivities is the secondary invariance conditions, which are simplified and then differentiated with respect to s to give relationships between the model sensitivities. This results in fairly crude approximations, but they have been found to be effective in previous work. The theory suggests a variety of means for improving these approximations, up to and including solving differential equations for the sensitivities as part of the numerical computation.

The starting point is the secondary invariance condition involving the total kinetic energy:

$$\langle \mathbf{v} \cdot \mathbf{v}/2 + k \rangle_s = 0. \tag{7}$$

Dropping the Reynolds average yields a convenient relationship between the sensitivities $|\mathbf{v}|_s$ and k_s:

$$(|\mathbf{v}|^2/2 + k)_s = |\mathbf{v}| \cdot |\mathbf{v}|_s + k_s = 0. \tag{8}$$

Two sources of error have been introduced here. Clearly, dropping the Reynolds average is unjustified, though it can be argued the effect is less the smaller the blending parameter λ is (and thus the closer the resolved variables are to being RANS variables). It could even be argued that the most important contributions from the model sensitivities are toward the RANS side of the LES-RANS transition and so this approximation might not be quite so crude as it first appears.

The second source of error is more subtle and results from having implicitly swapped the order of averaging and differentiating. Considering the most basic form of the total kinetic energy helps to make this clear:

$$\text{total ke} = \frac{1}{2}(\mathbf{v} + \mathbf{v}')^2 = \frac{1}{2}\mathbf{v} \cdot \mathbf{v} + \mathbf{v}' \cdot \mathbf{v} + \frac{1}{2}\mathbf{v}' \cdot \mathbf{v}' = \frac{1}{2}\mathbf{v} \cdot \mathbf{v} + \mathbf{v}' \cdot \mathbf{v} + k + \left(\frac{1}{2}\mathbf{v}' \cdot \mathbf{v}' - k\right). \tag{9}$$

The resolved and unresolved (subgrid) velocities are $\mathbf{v}$ and $\mathbf{v}'$, respectively, and the final term (in parenthesis) on the right is the fluctuating part of the subgrid kinetic energy. Averaging this expression (using the average that distinguishes resolved from subgrid scales, not the Reynolds average) yields $|\mathbf{v}|^2/2 + k$ as expected, but if the expression is differentiated with respect to s first and then averaged, the final term on the right, the

subgrid fluctuation term, will, in general, make a contribution. Its function is to provide the transfer of fluctuations across the resolved/unresolved boundary and its inclusion in this analysis is what permits the present approach to systematically incorporate the addition and subtraction of fluctuations from the flow as appropriate during the transition between LES and RANS regions.

Before proceeding to the discussion of the subgrid fluctuation term and integrated turbulence generation, however, additional relations are required to completely define the model sensitivities. Equation 8 relates the velocity magnitude sensitivity and the modelled turbulent kinetic energy sensitivity. To determine the sensitivities k_s and ω_s, it is argued that the destruction terms in the k and ω equations are ultimately responsible for removing all the k or all the ω from the system, regardless of the value of the blending parameter, and thus the destruction term is itself a model invariant. This is, of course, a fairly dramatic simplification, but it has been effective in work to date. The result of these simplifications is one finds $\omega_s = 0$ and $k_s = -k(\ell_{\mathrm{RANS}}/\ell_{\mathrm{LES}} - 1)/(1 - \lambda + \frac{3}{2}\lambda\ell_{\mathrm{RANS}}/\ell_{\mathrm{LES}})$.

With k_s available, $|\mathbf{v}|_s$ may be computed from Equation 8 and only computation of the individual velocity component sensitivities remains to be specified. In general, the secondary model invariants for the momentum equations could be used to generate relations for each of the components, but here it will simply be assumed the magnitude of the velocity sensitivity is as given by Equation 8 and its direction is normal to the LES-RANS boundary (that is, it is in the direction of $\nabla\lambda$).

III.A.4. Integrated Turbulence Generation

It remains to consider the effect of the subgrid fluctuation term in Equation 8. The treatment of this term differs from that of the others discussed above in two ways: it requires subgrid information not contained in the original governing Equations 2 and it is handled differently depending on whether fluctuations are being added through movement into a more LES-like region (increasing λ) or whether fluctuations are being removed through movement into a more RANS-like region (decreasing λ).

The missing subgrid information may be supplied by expressions similar to those employed for specifying turbulent inflow conditions for LES and hybrid LES-RANS computations. Thus a contribution to the velocity field might be (after Ref. 32)

$$\Sigma_i \sigma_i q_i \cos(\alpha_i \cdot x - \beta_i t + \phi_i), \tag{10}$$

where the $\sigma_\mathbf{i}$ are solenoidal unit vectors in random directions, the q_i are scalar amplitudes that may be estimated on dimensional grounds, the α_i and β_i are wavenumber and frequency vectors representative of the boundary between the resolved and unresolved scales at the point in question and the ϕ_i are random phase shifts. It is important to note that here, unlike the case of specifying turbulent inflow conditions, only a small section of the turbulent spectrum must be represented and so many fewer modes are required.

Expressions like this serve to add fluctuations when required, but it is also necessary to remove fluctuations. This may be done by filtering, with the filter cutoff determined by the blending parameter so as to yield a level of fluctuations appropriate to the local value of the blending parameter. Of course, since the projection which determines this appropriate level has been defined only implicitly by the governing equations, the nature of the filter and the relationship between the cutoff and λ can only be an approximation.

Between expressions like Equation 10 and the filtering described in the previous paragraph, the fluctuations to be added or removed between s and $s + ds$ may be computed and the corresponding contribution to $\mathbf{v}_s$ and the other model sensitvities determined. However, there is a simpler way to implement these effects (presumably with some loss of accuracy), and the fact that fluctuations are both added and removed at any given point still has to be clarified. These issues are discussed next.

The effect of the subgrid fluctuation term may best be understood as operating on fluxes, rather than on the primary flow variables themselves. The purpose of this term is to modify the fluxes that appear in the governing equations so that the fluxes affecting the evolution of the variables at a point are at the same LES/RANS mix as the variables themselves. Thus, fluxes coming from the more LES-like side (larger values of the blending parameter) have more fluctuations than they should and the fluctuations at the resolved/unresolved margin need to be removed by the filtering operation described above. Similarly, fluxes coming from the more RANS-like side (smaller values of the blending parameter) have too few fluctuations and fluctuations at the margin need to be added according to Equation 10.

These effects are most clearly seen when convective terms are considered. If a flow sweeps turbulence from a RANS to an LES region, clearly fluctuations must be added as the fluid passes through the LES/RANS transition. On the other hand, if turbulence is being swept from an LES region into a RANS region, than

fluctuations must be removed during the RANS/LES transition. By recognizing that the effects just described dominate those associated with the other terms in the governing equations, the numerical implementation of the subgrid fluctuation term may be simplified so that fluctuations are only added in the upstream, top and bottom boundaries of the LES box and only removed in the downstream boundary. (The choice for the bottom was based on the fact the mean normal velocity in a growing boundary layer is directed away from the wall. The choice for the top is a guess, made with the confidence inspired by the fact the modelled kinetic energy is so low at the top transition zone the choice doesn't matter much anyway.)

Further simplification is possible by recognizing that, at this stage in the development of this approach, little is known about the appropriate distribution of modes in the expression of Equation 10 for generating fluctuations. Good semi-empirical representations of the spectrum for fully developed turbulence are certainly available[32] and should provide bases for better approximations in the future, but, for the present, it has been found sufficient to use a set of modes with a single streamwise wavenumber set by the turbulent length scale ℓ_{RANS} (intended to be an estimate of the length scale at the boundary between resolved and unresolved scales), a single frequency determined so the phase speed is equal to the freestream velocity and a set of spanwise wavenumbers equal to those used in the spanwise spectral discretization of the code. These modes have equal amplitude.

Before setting the overall amplitude of the modes, consider that the effect of the subgrid fluctuation term in Equation 8 is to add terms like Equation 10 to model sensitivities like $\mathbf{v}_s$. The model sensitivities are then substituted in the new terms in the governing equations introduced by the derivatives of Equation 6 and the end result is that each governing equation has new terms of the form in Equation 10, with the amplitudes of the waves being the sum of the amplitudes of the individual terms in the equations. It is natural, then, given that the amplitude of the expression in Equation 10 is only estimated by dimensional analysis anyway, to suggest simply estimating the overall amplitude (by dimensional analysis) of the resulting forcing term in the governing equations and bypassing the intermediate steps. The amplitude of that forcing term is then $\propto k\ f(S/\omega, \ell_{RANS}, \ell_{LES}, \ldots)$; for the present computations, f is taken to be unity and the constant of proportionality is determined empirically.

The results presented below show that this fairly drastic approximation works reasonably well, but clearly there is much potential for improvement and the model-invariant formulation opens up significant opportunities: the function f in the dimensional analysis could be explored, the amplitude q_i in 10 could be estimated dimensionally in various ways and substituted in the individual model-invariance terms in the governing equations to give a more complex, but potentially more accurate, representation of the subgrid-fluctuation term than that employed here.

III.B. Hybrid Adaption

With the embedded-LES capability available, adaption is conceptually straightforward: one simply adjusts the position of the transition zones between LES and RANS regions until the solution is insensitive to further movement of those zones. In the case of the NASA hump, the LES box is placed in the separation bubble and is allowed to grow until the solution ceases to change.

The sensitivity of the solution to movement of the transitions zones is measured by an appropriate feature of the flow, preferably one which converges statistically fairly rapidly, in order to minimize the amount of computational time required during each stage of the adaption process. The position of the separation-bubble reattachment point fits this description and is used in the present computations.

Since the adaption process involves repeated computations of a flow, it is critical that the computations be made as efficient as possible. In addition to gauging sensitivity by means of quantities whose statistics converge rapidly, use is made of the fact that the determination to be made here, that of transition-zone positioning, is essentially qualitative and thus requires only qualitatieve levels of accuracy. Consequently, the adaption runs are made with the alternative Grid B mentioned above, providing a speedup by a factor of two, since the time step is governed by the smallest cell size. Runs are made for a period of $2c/u_\infty$, followed by an additional $2c/u_\infty$ for averaging, instead of the longer $10c/u_\infty$ and $10c/u_\infty$ used for the Grid A computations of the original embedded LES configuration. This provides an additional speedup factor of five over a normal quantitative run. Organizing the adaption process as a series of relatively small increments may also be used to reduce transients from run to run. Once the adaption process is complete, a quantitative run may be made with normal gridding and normal averaging times.

III.C. Grid Adaption

The adaption of the grid is controlled by the hybrid-adaption process, with the local value of the blending parameter providing information as to how the resolution in each part of the grid is to be determined. The relative simplicity of the NASA hump geometry significantly restricts the efficiency gains possible through grid adaption: the resolution requirements normal to the walls are similar for RANS and LES, so there is little for adaption to do, and the statistical homogeneity in the spanwise direction implies uniform grid spacing, so there is little for adaption to do there either (other than increase or decrease the total number of grid points). This leaves the streamwise distribution of gridpoints, which may be adjusted throughout the adaption process to concentrate points in the LES region while leaving sufficient points in the RANS regions for an accurate solution.

The structured grid employed in these computations makes r-refinement the most appropriate scheme for grid adaption, so the process comes down to determining the desired resolution at each streamwise station and then computing a distribution of grid points that yields that resolution as closely as possible with a specified number of grid points. The desired resolutions for LES and RANS are based on the local strain rate, with the two blended using the hybrid blending parameter to yield the desired metric for the grid-adaption computation. The distribution of the points normal to the walls is that of Grid B, described earlier, and efforts to improve computational efficiency similar to those employed for hybrid adaption are employed here, as well.

IV. Results

Results will now be presented illustrating the effectiveness of the various components of the adaptive embedded LES computation. First, the results of a basic embedded LES computation will be presented, with the limits of the LES box specified before the computation. This computation is, of course, the essential enabler of all that follows. Second, an adaptive computation is presented. The adaption is only over the location and size of the LES box; the same grid used in the first embedded LES computation is employed throughout this computation. Third, results involving adaptive gridding are presented. The adaptive gridding scheme described above is employed and the number of streamwise gridpoints is fixed to the number employed in the grid used in the previous computations.

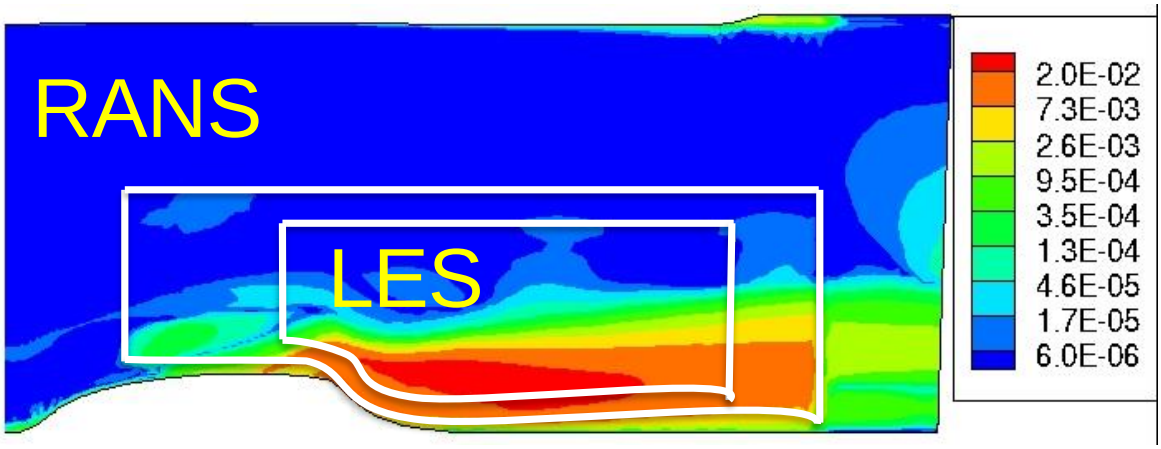

Figure 2. Resolved Reynolds shear stress ($\langle u'v' \rangle / u_\infty^2$) from embedded-LES computation. Colors are assigned logarithmically.

IV.A. Embedded LES

The basic capability to perform embedded LES is demonstrated with a computation with the inflow LES box boundary occupying the interval $x/c = 0.3$ to $x/c = 0.5$ and the the outflow boundary on the interval

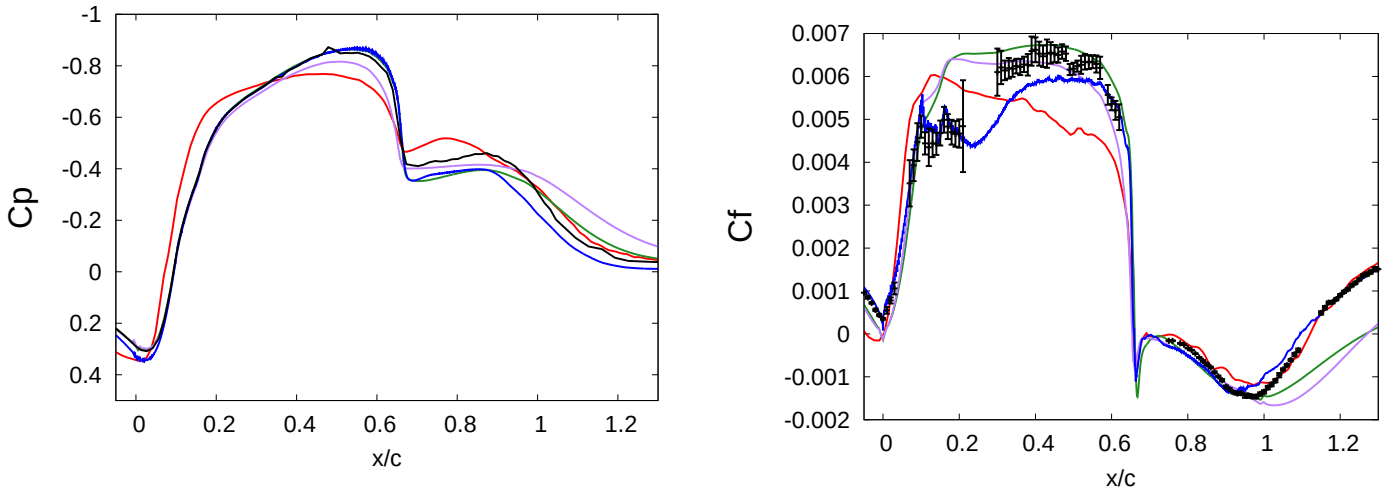

Figure 3. Pressure coefficient (left) and skin friction (right) from embedded-LES computations. The present embedded-LES results are shown in red, the experimental data points are in black. Also shown are results available on TMR:[33] wall-resolved LES,[24] blue; Menter SST RANS, green and Spalart-Almaras RANS, purple.

$x/c = 1.5$ to $x/c = 1.7$. The resolved Reynolds shear stress, $\langle u'v' \rangle / u_\infty^2$, where u' and v' are the fluctuating velocities (with respect to the Reynolds average) in the streamwise and normal directions and u_∞ is the inflow velocity, is shown in Figure 2. Note that colors are assigned logarithmically, so the full range from blue to red represents almost four orders of magnitude. This range is exhibited at the inflow transition zone ($x/c = 0.3$ to $x/c = 0.5$), where the ability of the present scheme to ramp the level of fluctuations up as required is demonstrated. Similarly, at the outflow transition zone, LES fluctations are ramped down several orders of magnitude as the flow enters the RANS region.

The accuracy of the results is confirmed by the comparison of the computed pressure coefficient and skin friction with the experimental data in Figure 3. Results from the Turbulence Modeling Resource[33] are also shown: the wall-resolved LES of Uzun et al.,[24] RANS with the Spalart-Almaras model and RANS with the Menter SST model.[33] (The latter model, of course, is the basis for the present blended hybrid model.) As is typical of most RANS for this and similar problems, reattachment occurs a significant distance downstream of the experimentally observed reattachment point. The wall-resolved LES and the present results are much closer.

The present results show reduced suction at the suction peak, which has been traced to a curious tendency for the blended model to produce high levels of turbulent viscosity at the outer edge of the boundary layer in high-speed, low-pressure regions. This is an example of the need for improved blended models mentioned above. The pressure is somewhat low in the separation region, the result of a loss of mean momentum in the LES-RANS transition. This is an artifact of the addition of fluctuations at the inflow LES-RANS boundary and is being investigated; it is not seen in model-invariant computations employing DES or wall-modelled LES configurations, such as that of Ref. 7. These anomalies also affect the skin friction on the forward part of the hump, but the computation recovers to yield accurate skin-friction predictions at and downstream of separation. A further anomaly brought out by the skin-friction comparison is the prediction difficulty produced by relaminarization over the forward quarter of the hump. Only the wall-resolved LES captures the relaminarization properly, but the RANS computations, while inaccurate in the relaminarization region, do recover rapidly and give good predictions for the skin friction in the middle and aft portions of the hump. The present computation fails to predict the skin friction in the relaminarization region and does not recover until the vicinity of the separation point is reached. This is a consequence of the close coupling between RANS and LES turbulence achieved by the model-invariant formulation: the incorrect, unrelaminarized, flow features in the RANS region are faithfully transferred to the LES region, making recovery more difficult.

Mean velocity and resolved Reynolds-stress profiles in and downstream of the mean separation bubble are shown in Figures 4–7. In addition to the present embedded-LES results, these figures include the

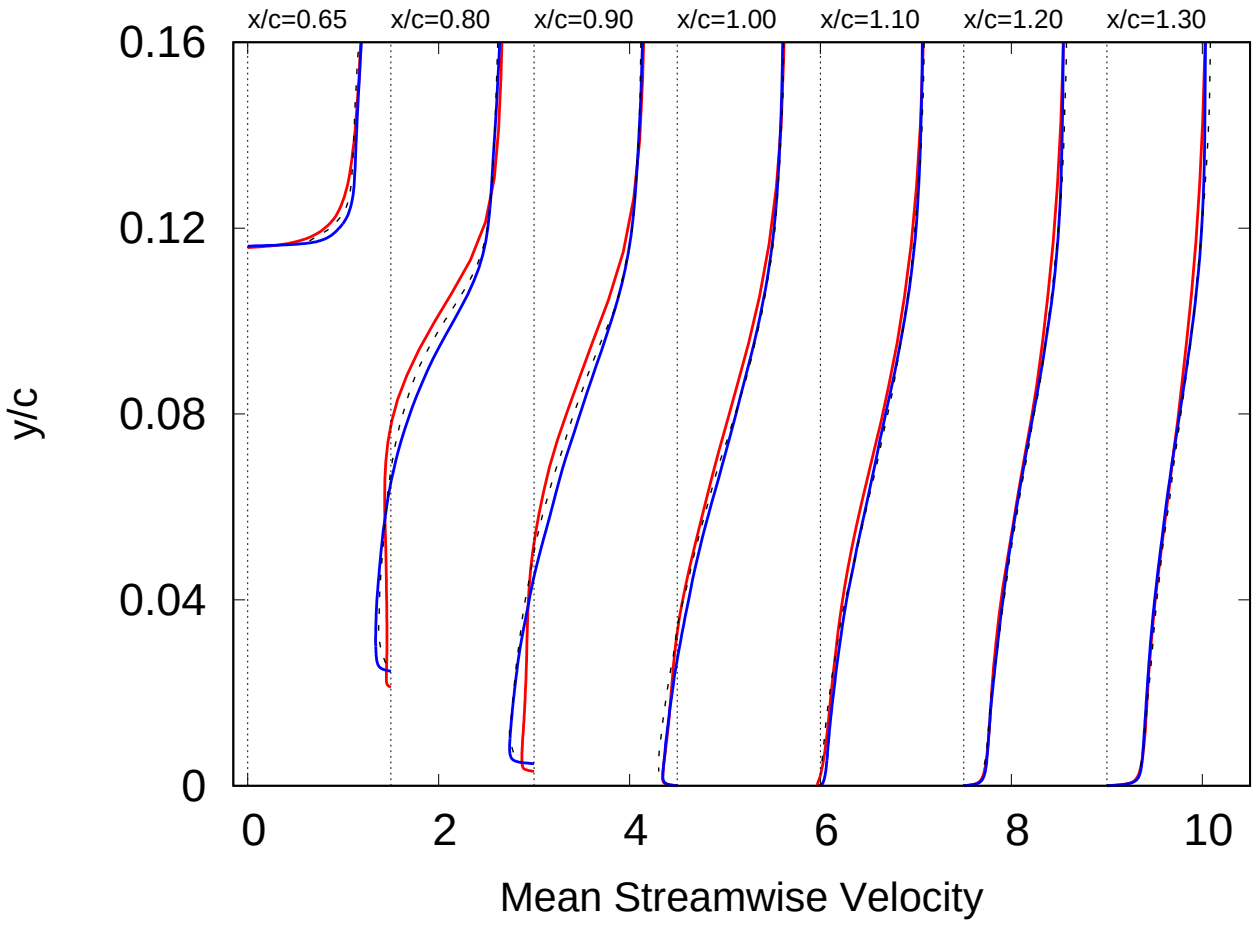

Figure 4. Mean velocity from embedded-LES computation, red; wall-resolved LES,[24] blue; experiment, black. Successive streamwise stations are shifted $1.5u_\infty$.

experimental PIV results and those from the wall-resolved LES of Uzun et al.[24] The dominant feature of the mean-velocity profiles (Figure 4) is the failure of the present results to reach proper levels in the separation bubble; this is a further consequence of the momentum loss at the inflow RANS-LES transition discussed above. Recovery from this problem occurs in the downstream portion of the separation bubble and the velocity profiles thereafter agree well with those of the experiment and of the wall-resolved LES. The embedded-LES resolved Reynolds-stress ($\langle u'v' \rangle$) profiles of Figure 5 exhibit excess fluctuations within the separation bubble, which seems to be associated with the mean-velocity and pressure issues already noted: the conversion from RANS to LES quantities in the inflow transition zone has resulted in both diminshed mean velocities and some excess fluctuations. As in the case of the mean-flow anomaly, there is some recovery of the Reynolds stress at downstream stations, but, in this case, Reynolds-stress magnitudes are too large near the separation streamline throughout the downstream section of the flow. On the other hand, the present results are actually better near the wall than the wall-resolved LES in the aft portion of the separation bubble and downstream of reattachment. The streamwise Reynolds stress ($\langle u'u' \rangle$, Figure 6) and the vertical Reynold stress ($\langle v'v' \rangle$, Figure 7) also exhibit excess fluctuations.

While there is no question the wall-resolved LES results of Uzun et al.[24] are more detailed and accurate than the present results, it is worth noting that computation was performed on a grid of 3×10^8 points. In contrast, the embedded LES required 4×10^4 points $\times$ 20 spectral modes. This represents a reduction in problem size of two and a half orders of magnitude. That the embedded-LES results are in many respects

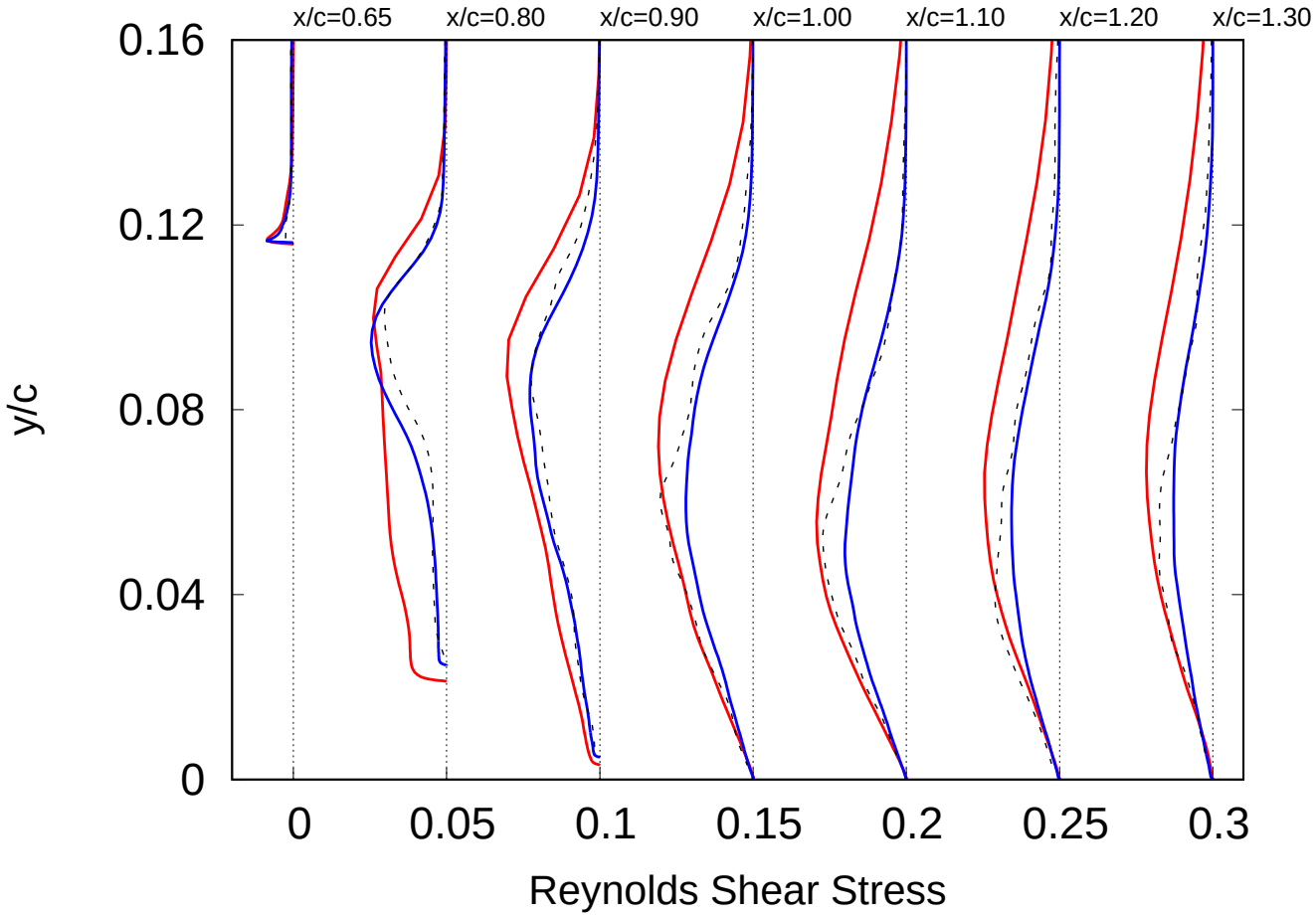

Figure 5. Reynolds shear stress ($\langle u'v' \rangle / u_\infty^2$) from embedded-LES computation, red; wall-resolved LES,[24] blue; experiment, black. Successive streamwise stations are shifted $0.05u_\infty^2$.

broadly comparable in accuracy to the wall-resolved LES thus already makes it an appealing alternative for many applications; this new technology's many avenues for development promise to make it even more appealing in the future. Eliminating some of the simplifications described above will be a start.

IV.B. Adaptive Embedded LES and Adaptive Embedded LES with Grid Adaption

Figure 8 shows a sequence of stages in the adaption process, beginning with the LES box entirely within the separation bubble and ending when the boundaries of the LES box are sufficiently outside the separation region that further changes have little effect on the results. The inflow and outflow boundaries are indicated by vertical black bars. In all cases, the lower boundary occupies the range $y/c = 0.01$ to $y/c = 0.1$ and the upper boundary the range $y/c = 0.4$ to $y/c = 0.6$. The changes from a) to b) and b) to c) are dramatic, both in the resolved Reynolds shear stress shown in the left column and in the mean velocity shown in the right column. The change in the LES box between c) and d) naturally still yields changes in the resolved shear stress on the left, but the mean velocity on the right changes very little, indicating a stable solution has been reached and the adaption process may stop.

A sequence of hybrid-adaption steps, this time paired with the distribution of grid spacings produced by the grid-adaption algorithm, is shown in Figure 9. While the changes in positioning of the LES box, and in the corresponding grids, are significant, results such as the mean velocity (not shown) are essentially

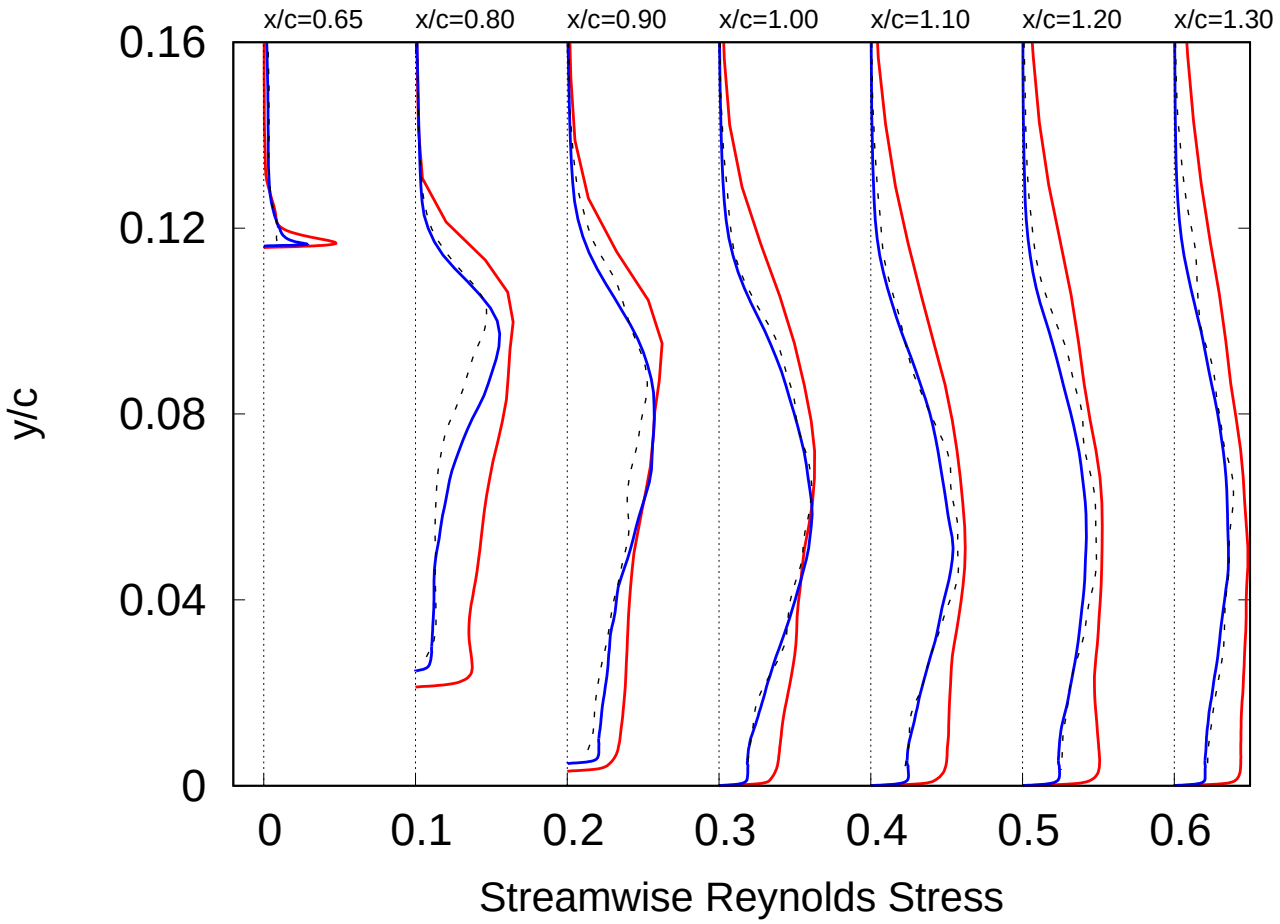

Figure 6. Streamwise Reynolds stress ($\langle u'u' \rangle / u_\infty^2$) from embedded-LES computation, red; wall-resolved LES,[24] blue; experiment, black. Successive streamwise stations are shifted $0.1u_\infty^2$.

unchanged and are indistinguishable from those in c) and d) of Figure 8. The grid of c) in Figure 9 is unexpectedly coarse in the front quarter of the airfoil, even though the RANS-LES transition begins there, because the coarsening due to low strain rates in that region dominates the refinement due to the RANS-LES transition in the grid metric formula.

Choosing d) of Figure 8 as the final stage of the hybrid-adaption computations and case c) of Figure 9 as representative of the grid-adaption computations, it may be seen in Figure 10 that these computations yield results broadly similar to those of the original embedded LES computation. The most dramatic difference is in the grid-adaption computation at the nose of the hump ($x/c \approx 0$) where C_p and C_f depart significantly both from the other computations and from the experiment. This is due to the extreme coarsening of the grid near the nose of the hump, which is, in turn, caused by the low strain rate there. Also of interest is the manner in which grid adaption improves the prediction of C_f over that of the pure hybrid-adaption computation for $x/c > 1$.

The profiles of the mean velocity and Reynolds stresses of Figures 11–14 also show results broadly similar to those of the original embedded LES, again with grid adaption sometimes improving the results and sometimes making them worse. In each figure, hybrid-adaption and hybrid- and grid-adaption results are shown together with those of the experiment and of the original embedded LES. The mean velocity profiles of Figure 11 exhibit little difference between the three computations, though there are a few places

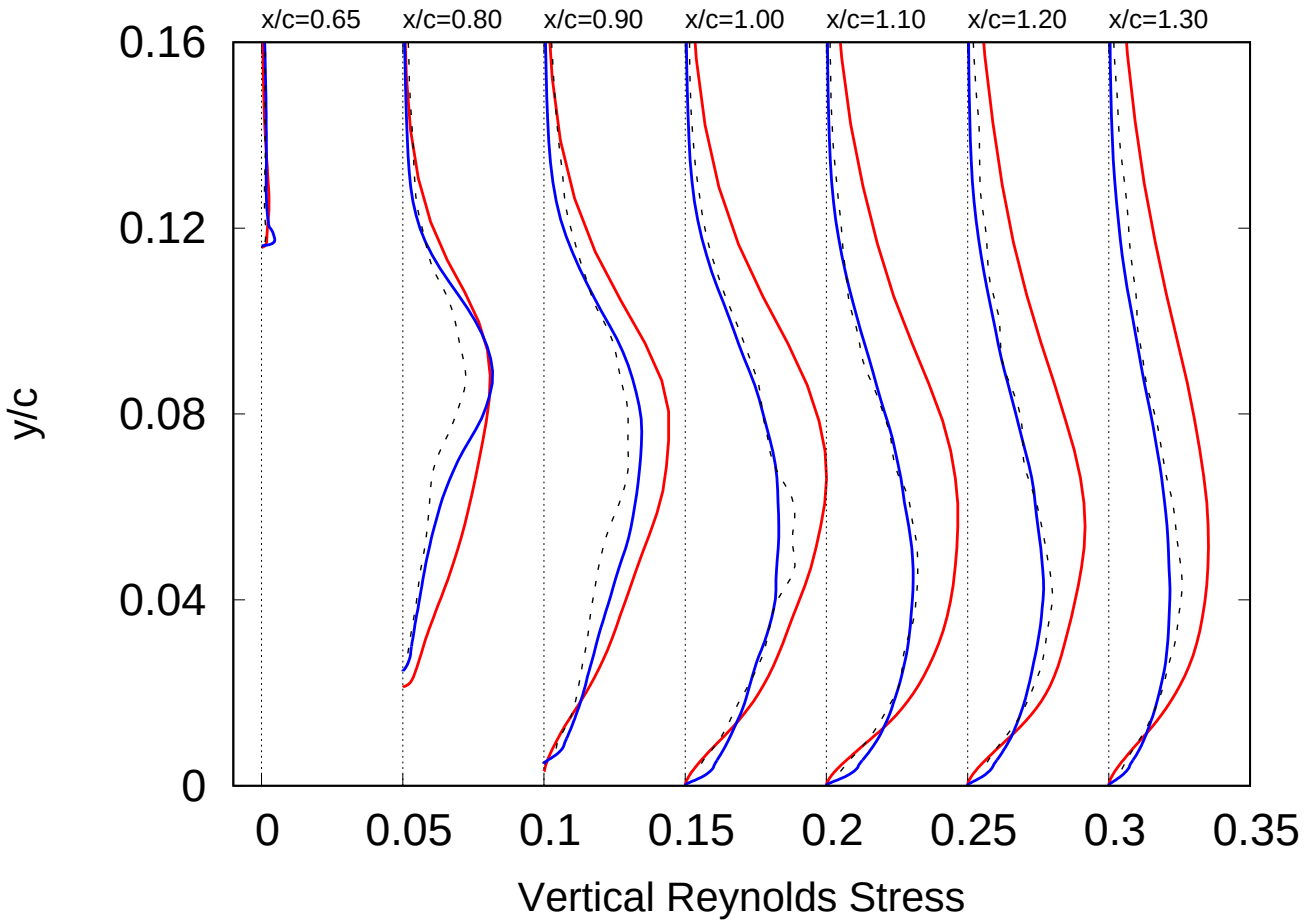

Figure 7. Vertical Reynolds stress ($\langle v'v' \rangle / u_\infty^2$) from embedded-LES computation, red; wall-resolved LES,[24] blue; experiment, black. Successive streamwise stations are shifted $0.05u_\infty^2$.

(the $x/c = 1.20$ profile near the wall, for example) where the hybrid-adaption computation deviates from the original embedded LES and the hybrid- and grid-adaption computation brings it back. The resolved Reynolds stresses show more significant differences. The Reynolds shear stress (Figure 12) is captured nearly as well by the hybrid-adaption computation as by the original embedded LES, but the hybrid- and grid-adaption computation tends to deviate in the mixing layer. This latter tendency is even more pronounced in the streamwise Reynolds stress (Figure 13) and the hybrid-adaption predictions are less accurate as well. Similar behavior is seen in the predictions of the vertical Reynolds stress (Figure 14).

That the qualitative adaptive computations agree to this extent with the original quantitative embedded LES, in spite of the reduced resolution and averaging run times, provide encouragement that this type of hybrid-adaption procedure, potentially paired with grid adaption, algorithm adaption, model adaption, etc., can be a cost-effective approach to automated hybrid computations. However, it is to be emphasized that these intermediate computations with reduced resolution, etc., are only qualitative and only used to guide the hybrid- and grid-adaption process. Once this process is complete, a fully quantitative computation, with appropriate resolution and averaging times, would be run to give the final result.

Finally, it is of interest to examine the grid-adaption process more closely for a representative case, say case a) of Figure 9. The streamwise distribution of mean strain Sc/u_∞ is shown in a) of Figure 15, along with the streamwise distribution of grid sizes Δ/c in b). The distribution of mean strain is largely as one

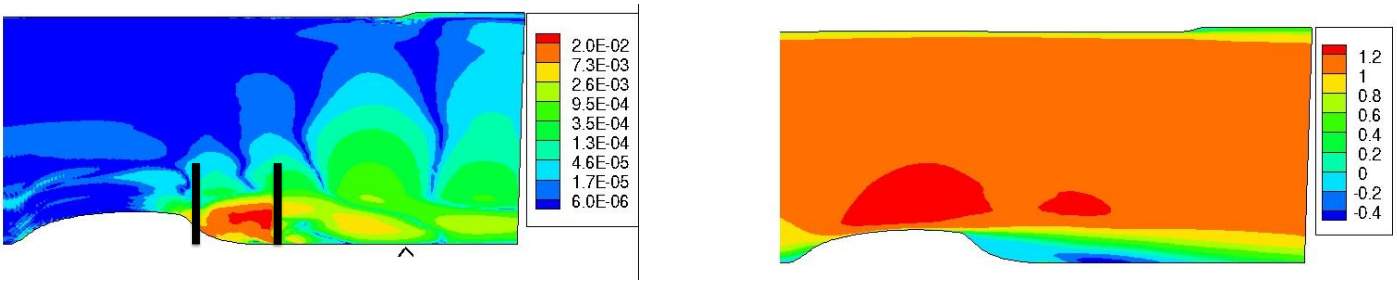

a) LES box inside separation bubble.

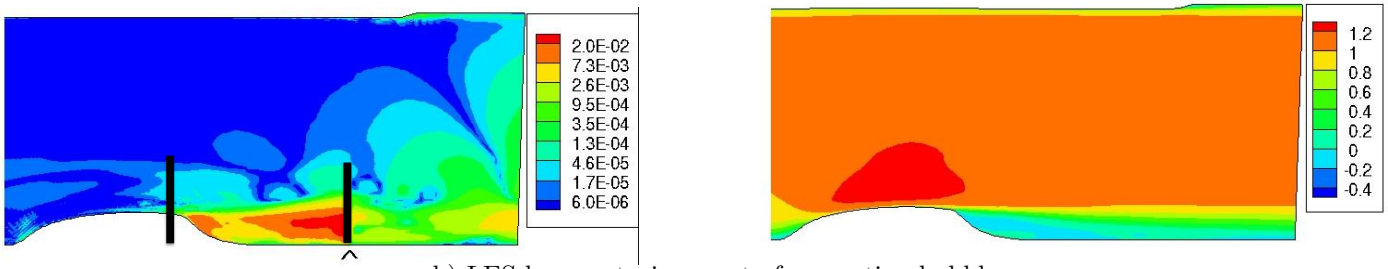

b) LES box capturing most of separation bubble.

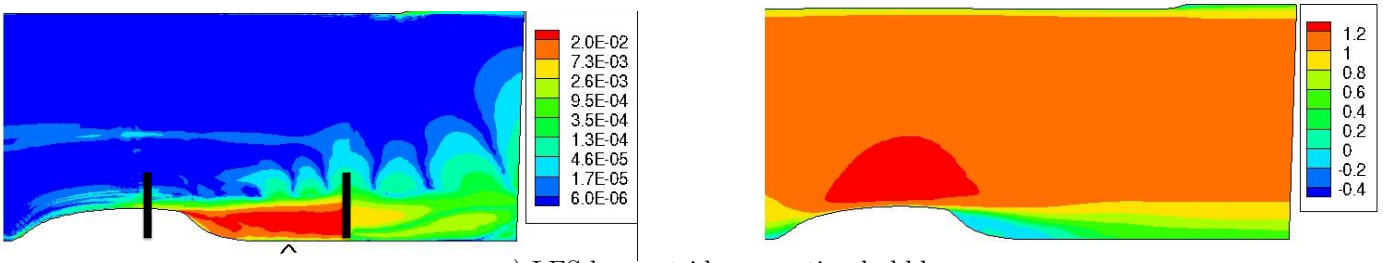

c) LES box outside separation bubble.

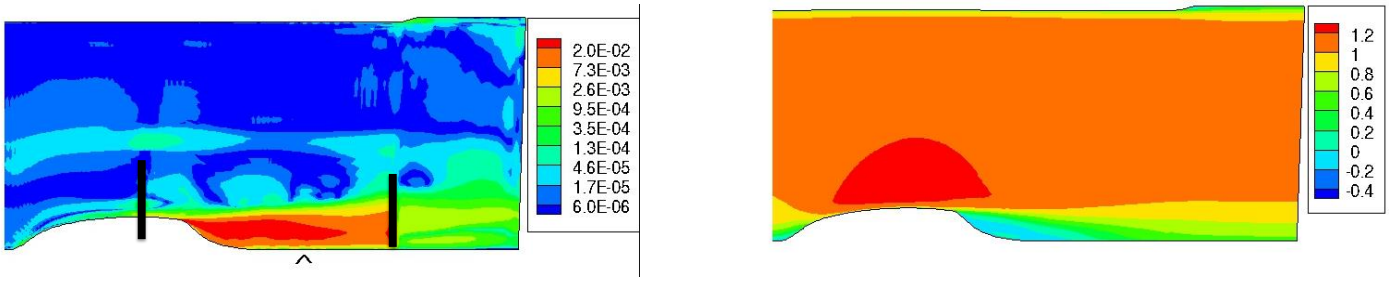

d) LES box further outside separation bubble.

Figure 8. Sequence of computations showing hybrid adaption. Contour plots in left column show resolved Reynolds shear stress ($\langle u'v' \rangle / u_\infty^2$); the vertical black bars indicate streamwise extent of the LES box and the carat indicates the reattachment point. Plots in right column show streamwise mean velocity; the blue area in the lee of the airfoil is the reversed-flow region and indicates the extent of the separation bubble.

would expect. (This is the peak value of the strain at a given x station, excluding values very near the wall, which would by dominated by $\partial u/\partial y$.) The distribution of grid sizes is computed with moderately aggressive smoothing and limiting to yield a solver-friendly grid. Adjustments to the various parameters defining this

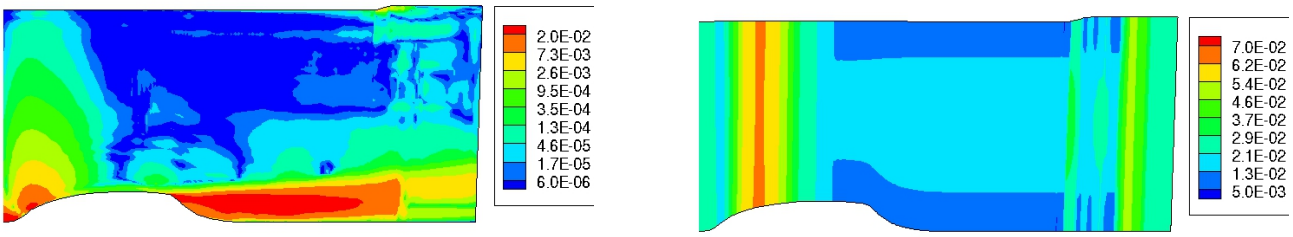

a) Inflow boundary of LES box just upstream of separation.

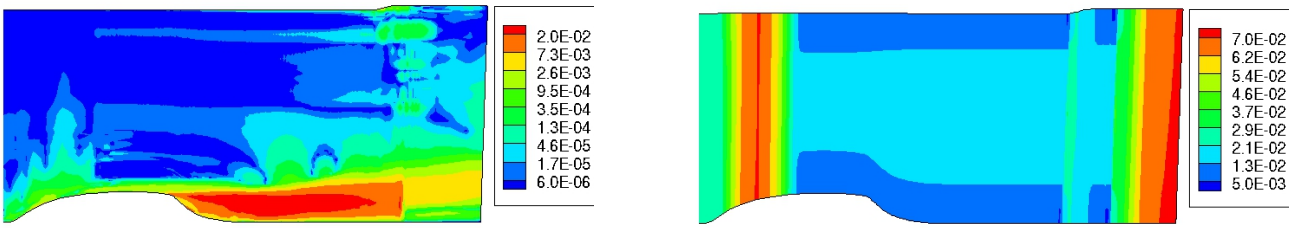

b) Inflow boundary of LES box at mid airfoil.

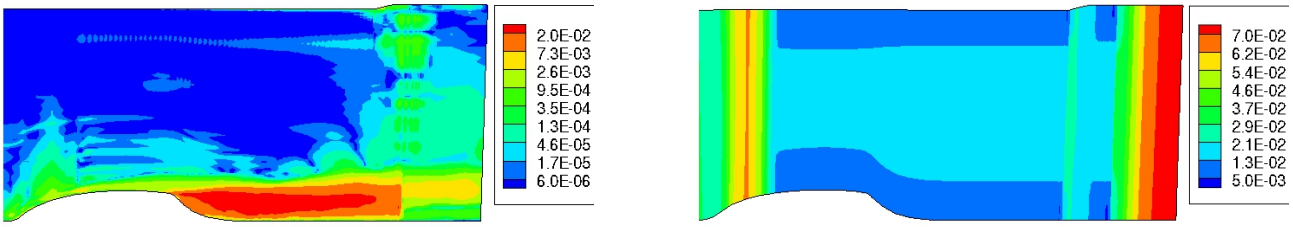

c) Inflow boundary of LES box at first quarter of airfoil.

Figure 9. A sequence of computations showing grid adaption. Contour plots in left column show resolved Reynolds shear stress ($\langle u'v' \rangle / u_\infty^2$); those in right column show distribution of longest grid side (usually $\Delta x/c$, except in center of plot, where $\Delta y/c$ is slightly larger). Inflow (left) boundary of LES box at three locations on airfoil; outflow (right) boundary at same location downstream of reattachment.

process are suggested by the excessive coarsening at the nose and other unphysical features just discussed.

V. Conclusion

The ability to perform embedded LES opens up an enormous range of possibilities for faster and more accurate computations of turbulent flows. One example is adaptive computations, in which the boundaries of the LES "box" automatically adapt to the requirements of the particular flow being computed. With this capability in place, additional adaptive technologies, such as grid adaption, algorithm adaption and adaption of the turbulence model can be tied to it. A demonstration of this capability has been presented in this paper, with successful embedded LES computations involving fixed grid and LES boundaries, fixed grid and adaptive LES boundaries and, finally, adaptive grid and LES boundaries.

The reduced grid resolution and computation averaging times for the qualitative adaptive computations worked well for the present test case, indicating the potential for significant cost savings (a factor of ten, as implemented here), particularly in the early stages of an adaptive computation. This is critical for an adaptive hybrid computation, given the number of computations required during the adaption process and the costliness of normal quantitative runs.

There are many opportunities for further development: this demonstration is a proof of concept only. As

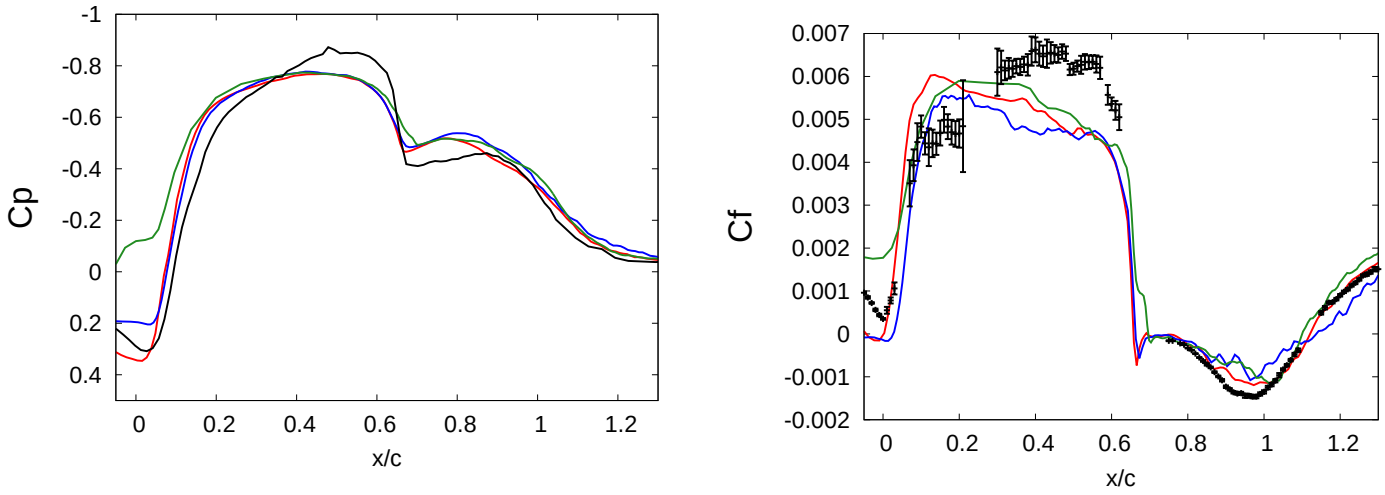

Figure 10. Pressure coefficient (left) and skin friction (right) from adaptive computations. Original embedded-LES computation, red; hybrid-adaption computation, blue; hybrid- and grid-adaption computation, green; experiment, black.

detailed above, extensive simplifications to the approximations of the model sensitivities and their implementation were employed in the present work; removing these simplifications and improving the approximations promises even more accurate and efficient computations.

The enabling technology for this work is the model-invariant hybrid formulation, which provides a depth of understanding of the dynamics of the LES-RANS transition not previously available. Most significant, of course, is the recognition of the importance of the modifications to the derivatives in the governing equations, without which model invariance cannot be satisfied and the physical significance of even the most basic averages is lost. The identification of the secondary model invariants introduces a new tool with many uses: their use, demonstrated here, for deriving approximations to the model sensitivities, their use as a means of assessing the validity of blended hybrid turbulence models, etc. The ability now to systematically distinguish between turbulence modeling effects and effects due to the LES-RANS transition will help keep model development from being led astray by incorrectly attibuting transition effects to the model.

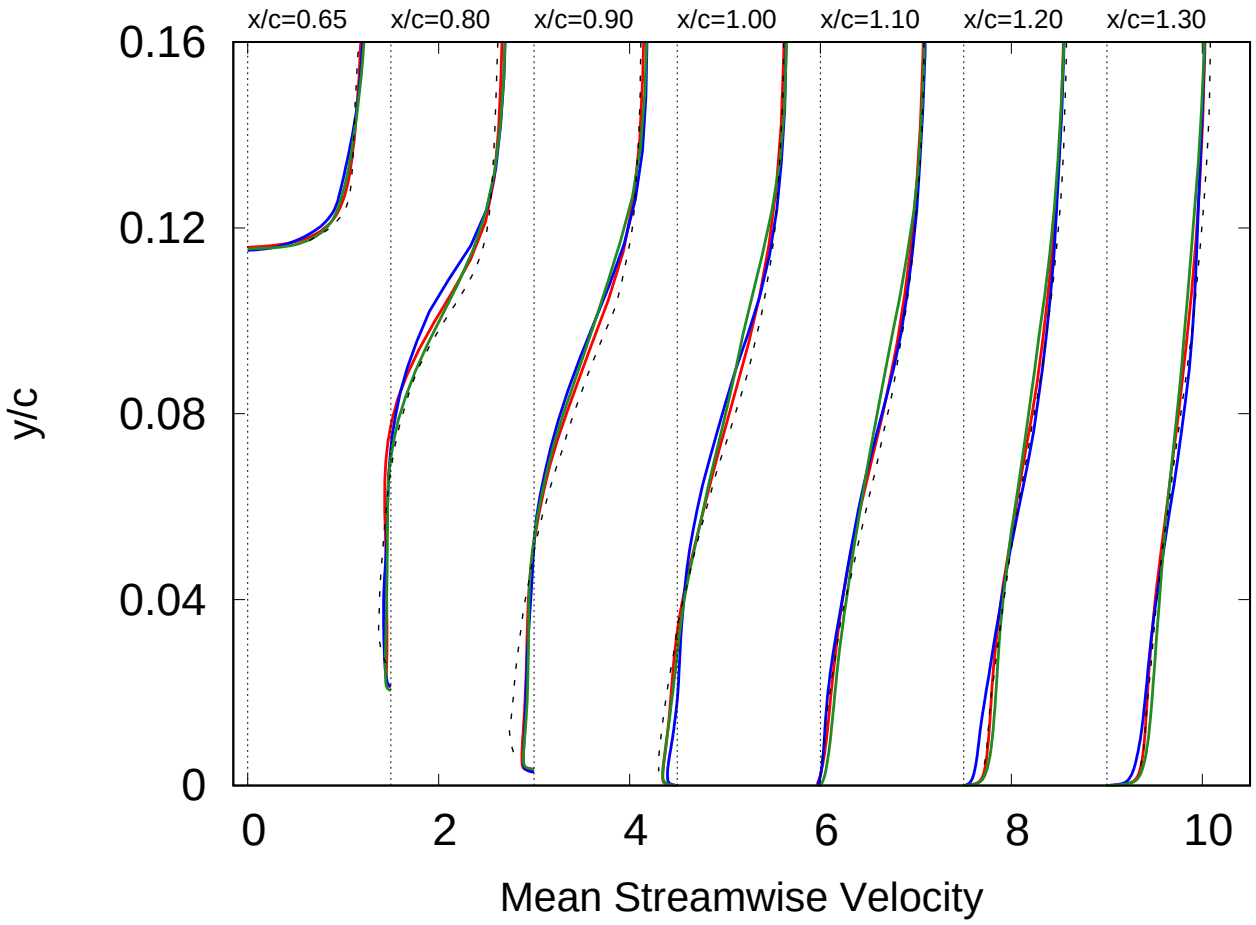

Figure 11. Mean velocity from adaptive computations. Original embedded-LES computation, red; hybrid-adaption computation, blue; hybrid- and grid-adaption computation, green; experiment, black. Successive streamwise stations are shifted $1.5u_\infty$**.**

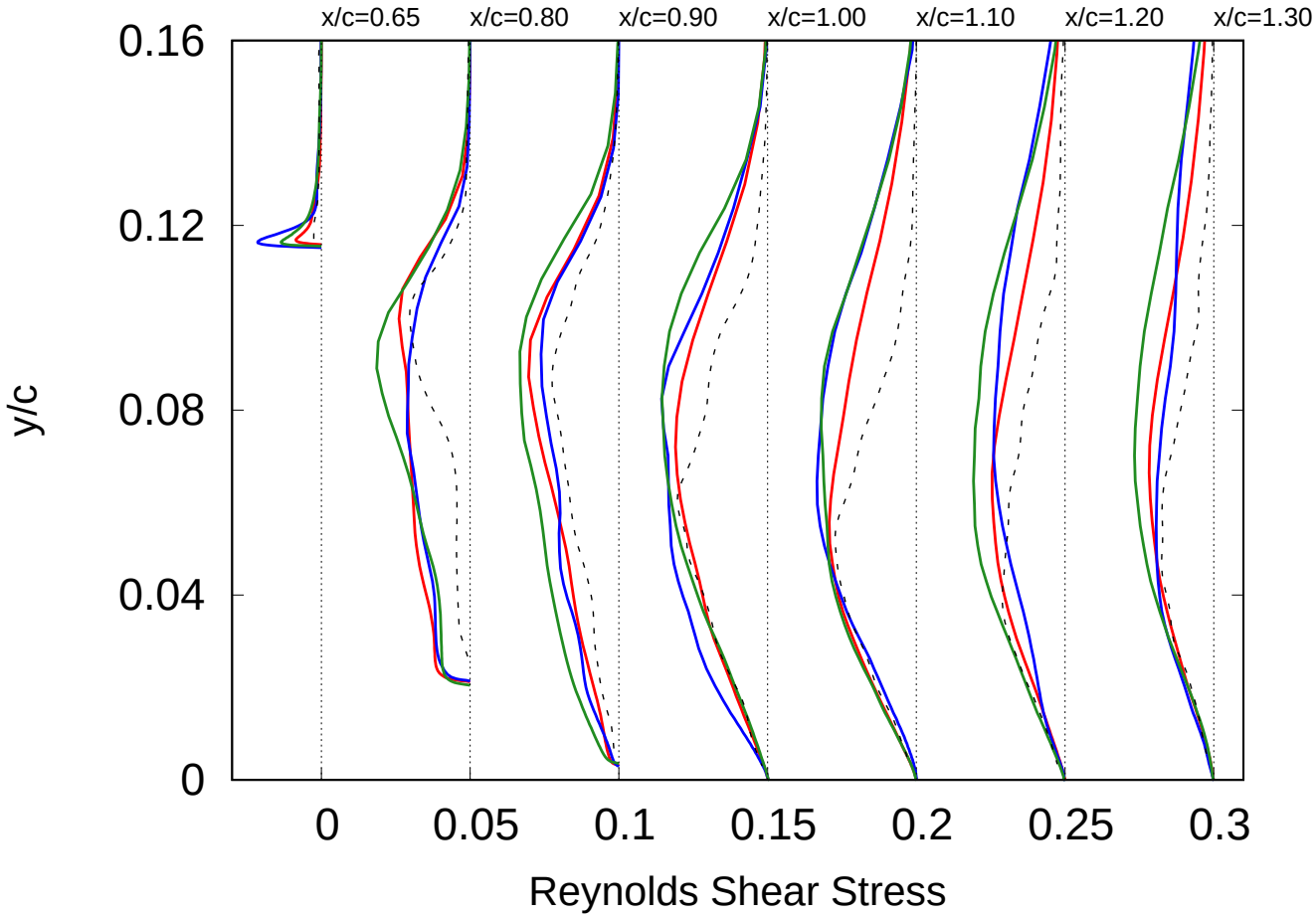

Figure 12. Reynolds shear stress ($\langle u'v' \rangle / u_\infty^2$) from adaptive computations. Original embedded-LES computation, red; hybrid-adaption computation, blue; hybrid- and grid-adaption computation, green; experiment, black. Successive streamwise stations are shifted $0.05u_\infty^2$.

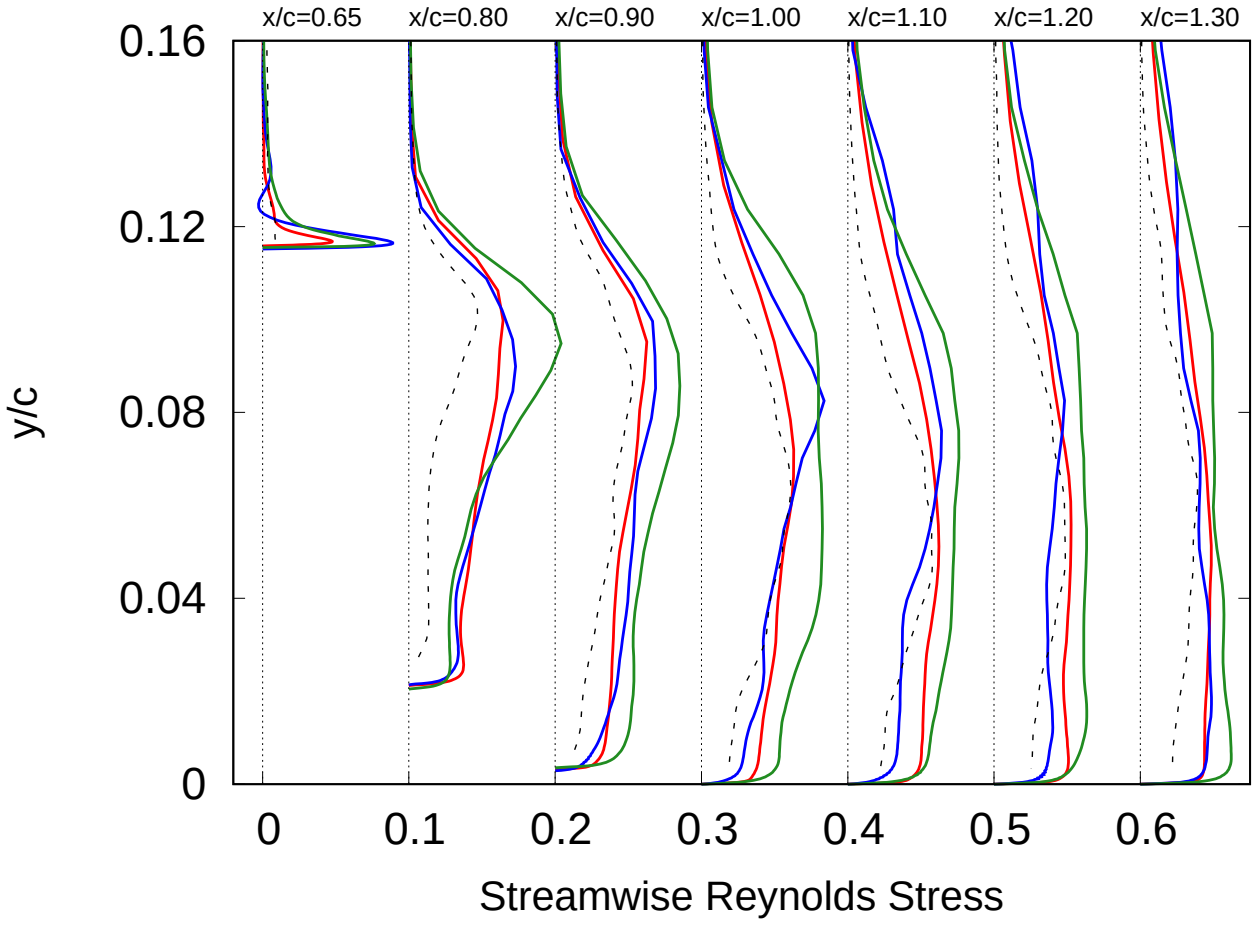

Figure 13. Streamwise Reynolds stress ($\langle u'u' \rangle / u_\infty^2$) from adaptive computations. Original embedded-LES computation, red; hybrid-adaption computation, blue; hybrid- and grid-adaption computation, green; experiment, black. Successive streamwise stations are shifted $0.1u_\infty^2$.

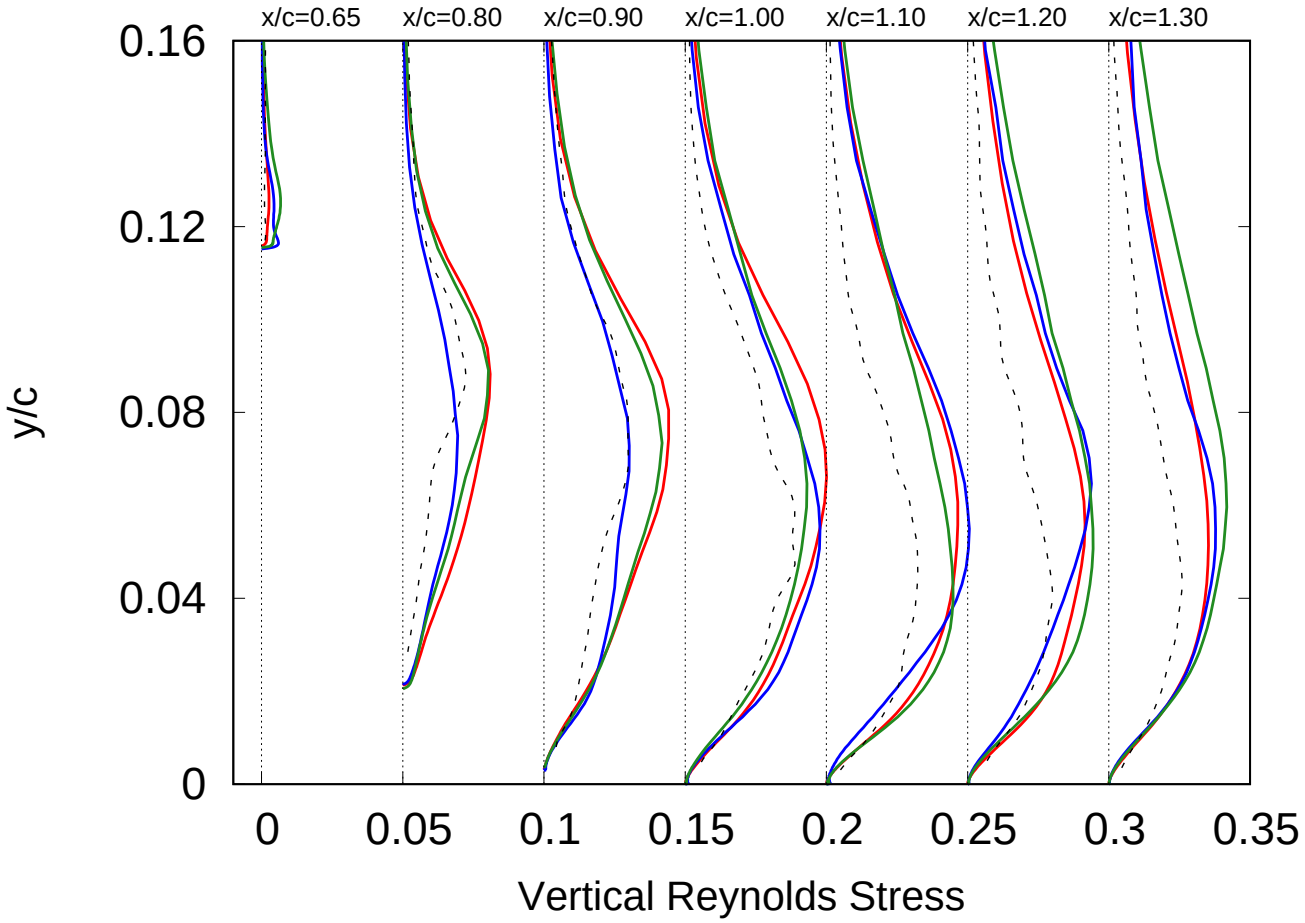

Figure 14. Vertical Reynolds stress ($\langle v'v' \rangle / u_\infty^2$) from adaptive computations. Original embedded-LES computation, red; hybrid-adaption computation, blue; hybrid- and grid-adaption computation, green; experiment, black. Successive streamwise stations are shifted $0.05u_\infty^2$.

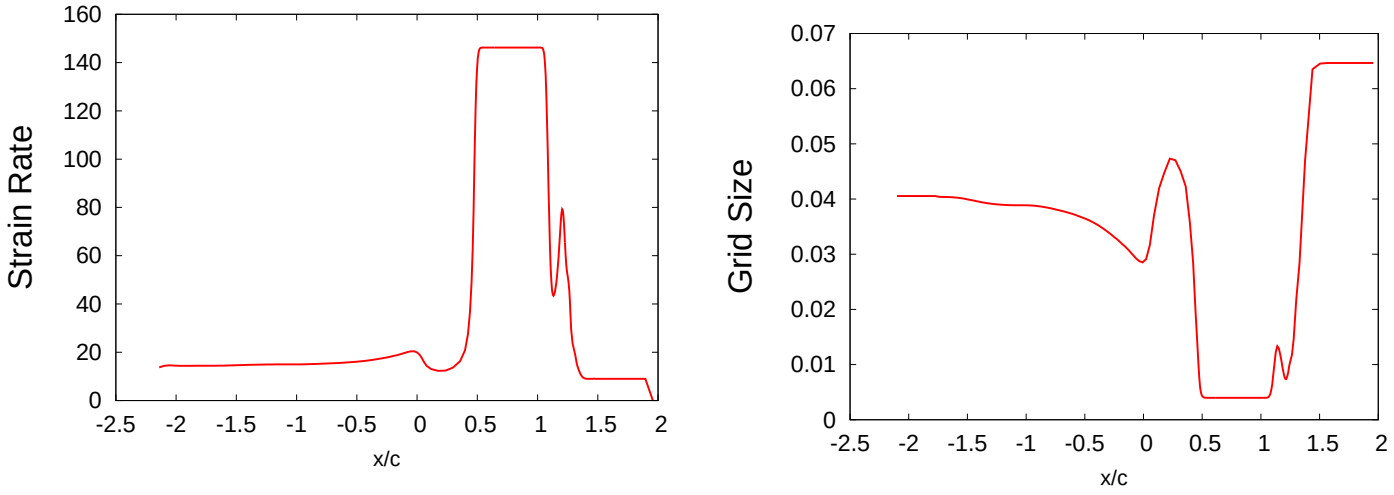

Figure 15. Streamise distribution of strain Sc/u_∞ (left) and grid size Δ/c (right) for adapted grid from a) of Figure 9.

References

[1]Spalart, P. R., "Detached-Eddy Simulation," *Annual Review of Fluid Mechanics*, Vol. 41, 2009, pp. 181–202.

[2]Cabot, W. and Moin, P., "Approximate wall boundary conditions in the large-eddy simulation of high Reynolds number flow," *Flow, Turbulence and Combustion,* Vol. 63, Nos. 1–4, 2000, pp. 269–291.

[3]Spalart, P., Belyaev, K., Garbaruk, A., Shur, M., Strelets, M., and Travin, A., "Large-Eddy and Direct Numerical Simulations of the Bachalo-Johnson Flow with Shock-Induced Separation," Eleventh International ERCOFTAC Symposium on Engineering Turbulence Modeling and Measurements, Palermo, Italy, September 2016.

[4]Woodruff, S. L., "Coupling Turbulence in Hybrid LES-RANS Techniques," *Seventh International Symposium on Turbulence and Shear-Flow Phenomena*, Ottawa, Canada, July 28–31, 2010.

[5]Woodruff, S. L., "A New Formulation for Hybrid LES-RANS Computations," 21st AIAA Computational Fluid Dynamics Conference, June 24-27, 2013, San Diego, CA, AIAA Paper 2013-2722.

[6]Woodruff, S., "Model-Invariant Hybrid LES-RANS Computation of Separated Flow Past Periodic Hills," in *Progress in Hybrid RANS-LES Modelling*, S. Girimaji et al. (eds.), *Notes on Numerical Fluid Mechanics and Multidisciplinary Design*, Vol. 130, Springer, 2015.

[7]Woodruff, S. L., "Model-Invariant Hybrid Computations of Separated Flows for RCA Standard Test Cases," 54th AIAA Aerospace Sciences Meeting, Jan. 2016, San Diego, CA, 2016-1559.

[8]Batten, P., Goldberg, U. and Chakravarthy, S., "LNS — An Approach Towards Embedded LES," 40th AIAA Aerospace Sciences Meeting, Jan. 2002, 2002-0427.

[9]Greenblatt, D., Paschal, K. B., Yao, C.-S., Harris, J., Shaeffler, N. W., and Washburn, A. E., "Experimental Investigation of Separation Control, Part 1: Baseline and Steady Suction," *AIAA Journal*, Vol. 44, No. 12, 2006, pp. 2820–2830.

[10]Germano, M., "Properties of the Hybrid RANS/LES Filter," *Theoretical and Computational Fluid Dynamics*, Vol. 17, 2004, pp. 225–231.

[11]Sanchez-Rocha, M. and Menon, S., "The Compressible Hybrid RANS/LES Formulation Using an Additive Operator," *Journal of Computational Physics*, Vol. 228, 2009, pp. 2037–2062.

[12]Sanchez-Rocha, M. and Menon, S., "An Order-of-Magnitude Approximation for the Hybrid Terms in the Compressible Hybrid RANS/LES Governing Equations," *Journal of Turbulence*, Vol. 12, 2011, N16.

[13]Rajamani, B. and Kim, J., "A Hybrid-Filter Approach to Turbulence Simulation," *Flow Turbulence Combust.*, Vol. 85, 2010, pp. 421–441.

[14]Wallin, S. and Girimaji, S., "Commutation Error Mitigation in Variable-Resolution PANS Closure: Proof of Concept in Decaying Isotropic Turbulence," *6th AIAA Theoretical Fluid Mechanics Conference*, June 27–30, 2011, Honolulu, HI, AIAA Paper 2011-3105.

[15]Medic, G., Templeton, J. A., and Kalitzin, G., "A Formulation for Near-Wall RANS/LES Coupling," *International Journal of Engineering Science*, Vol. 44, 2006, pp. 1099–1112.

[16]Breuer, M., Jaffrezic, B., and Arora, K., "Hybrid LES-RANS Technique Based on a One-Equation Near-Wall Model," *Theoretical and Computational Fluid Dynamics*, Vol. 22, 2008, pp. 157–187.

[17]Wang, M. and Moin, P., "Dynamic wall modeling for large-eddy simulation of complex turbulent flows," *Physics of Fluids*, Vol. 14, No. 7, 2002, pp. 2043–2051.

[18]Shur, M. L., Spalart, P. R., Strelets, M. Kh. and Travin, A., "A hybrid RANS-LES approach with delayed-DES and wall-modeled LES capabilities," *Int. J. Heat and Fluid Flow*, Vol. 29, 2008, pp. 1638–1649.

[19]Choi, J.-I., Edwards, J. R. and Baurle, R. A., "Compressible Boundary Layer Predictions at High Reynolds Number using Hybrid LES/RANS Methods," *AIAA J.*, Vol. 47, No. 9, 2009, pp. 2179–2193.

[20]Gieseking, D. A., Choi, J.-I., Edwards, J. R. and Hassan, H. A., "Simulation of Shock/Boundary Layer Interactions Using Improved LES/RANS Models," *48th AIAA Aerospace Sciences Meeting*, January 4–7, 2010, Orlando, FL, AIAA Paper 2010-0111.

[21]Hamba, F., "Log-layer mismatch and commutation error in hybrid RANS/LES simulation of channel flow," *Int. J. Heat and Fluid Flow*, Vol. 30, 2009, pp. 20–31.

[22]Keating, A., De Prisco, G. and Piomelli, U., "Interface conditions for hybrid RANS/LES calculations," *Int. J. Heat and Fluid Flow*, Vol. 27, 2006, pp. 777–788.

[23]Pauley, L. L., Moin, P. and Reynolds, W. C., "The structure of two-dimensional separation," *Journal of Fluid Mechanics*, vol. 220, 1990, pp. 397–411.

[24]Uzun, A. and Malik, M. R., "Large-Eddy Simulation of Flow over a Wall-Mounted Hump with Separation and Reattachment," *AIAA J.*, Vol. 56, No. 2, 2018, pp. 715–730.

[25]Probst, A., Schwamborn, Garbaruk, A., Guseva, E., Shur, M., Strelets, M. and Travin, A., "Evaluation of grey area mitigation tools within zonal and non-zonal RANS-LES approaches in flows with pressure induced separation," *Int. J. Heat and Fluid Flow*, Vol. 68, 2017, pp. 237–247.

[26]Menter, F. R., "Two-Equation Eddy-Viscosity Turbulence Models for Engineering Applications," *AIAA J.*, Vol. 32, No. 8, 1994, pp. 1598–1605.

[27]Strelets, M., "Detached Eddy Simulation of Massively Separated Flows," *39th AIAA Aerospace Sciences Meeting*, January 8–11, 2001, Reno, NV, AIAA Paper 2001-0879.

[28]Visbal, M. R. and Gaitonde, D. V., "On the Use of Higher-Order Finite-Difference Schemes on Curvilinear and Deforming Meshes," *Journal of Computational Physics*, Vol. 181, 2002, pp. 155–185.

[29]CFL3D Version V Manual, http://cfl3d.larc.nasa.gov, last accessed April 30, 2013.

[30]Higuera, D., Sekhar, S., Mansour, N. N., Razi, P., and Girimaji, S., "PANS Simulations of Turbulent Separated Flow over a Wall-Mounted Hump," *22nd AIAA Computational Fluid Dynamics Conference*, 22–26 June 2015, Dallas, TX, AIAA Paper 2015-2463.

[31]Spalart, P. R. and Rumsey, C. L., "Effective Inflow Conditions for Turbulence Models in Aerodynamic Calculations," *AIAA J.*, Vol. 45, No. 10, 2007, pp. 2544–2553.

[32]Shur, M. L., Spalart, P. R., Strelets, M. K. and Travin, A. K., "Synthetic Turbulence Generators for RANS-LES Interfaces in Zonal Simulations of Aerodynamic and Aeroacoustic Problems," *Flow Turbulence Combust.*, Vol. 93, 2014, pp. 63–92.

[33]Rumsey, C. L., Turbulence Modeling Resource, http://turbmodels.larc.nasa.gov, last accessed November 16, 2018.